A Terahertz Micromachined On-Wafer Probe for WR-1.2 Waveguide

Matthew Bauwens, Lihan Chen, Chunhu Zhang, Alex Arsenovic,
Arthur Lichtenberger, N. Scott Barker, and Robert M. Weikle

Charles L. Brown Department of Electrical Engineering,
University of Virginia, Charlottesville, VA 22903, U.S.A.

***Abstract*—A micromachined on-wafer probe designed for WR-1.2 rectangular waveguide is demonstrated in this paper to further enable submillimeter-wave integrated circuits testing. Initial measurements of a prototype WR-1.2 micromachined on-wafer probe exhibit an insertion loss better than 9 dB for the lower half of the WR-1.2 band.**

I. Introduction

The terahertz frequency spectrum (300-3000 GHz) has been a subject of scientific research for many decades [1], and recent progress [2],[3] in the development of terahertz monolithic integrated circuits (TMICs) could open the door to many new applications. The development of such complex circuits relies on accurate device models, which are obtained most quickly and easily through on-wafer probing [4]. Commercially, on-wafer probes are available up to 500 GHz, and the recent development of an on-wafer probe for the WR-1.5 waveguide band [5], [6] has enabled on-wafer measurements up to 750 GHz [3]. Above 750 GHz, however, on-wafer probes do not exist, which requires that researchers use alternative testing methods. These methods often involve dicing out individual circuits to mount in a test fixture, which is inherently time consuming and may introduce additional errors associated with the test fixture.

To better facilitate the development of higher frequency TMICs, an on-wafer probe for the WR-1.2 waveguide band, which covers the 600-900 GHz frequency range, has been designed and fabricated based on the approach pioneered in [5] and [6]. As shown in Fig. 1, the on-wafer probe assembly consists of two parts. The first is an ultra-thin silicon chip that is microfabricated using the methods established in [7]. The second is a micromachined E-plane split-block waveguide housing, which is milled using conventional computer numerical control (CNC) machining techniques. It features milled recessions that both self-align the probe chip within the block and allow it to be clamped in place between the two block halves without the need for adhesives. In order to make contact with the device-under-test (DUT) on-wafer, the tip of the probe chip extends below the bottom of the waveguide block. As the probe tip is brought into contact with the wafer, the clamped areas hold it firmly in place, causing the tip to deflect and generate a force at the contact points. This paper presents the design and initial test results of the WR-1.2 on-wafer probe.

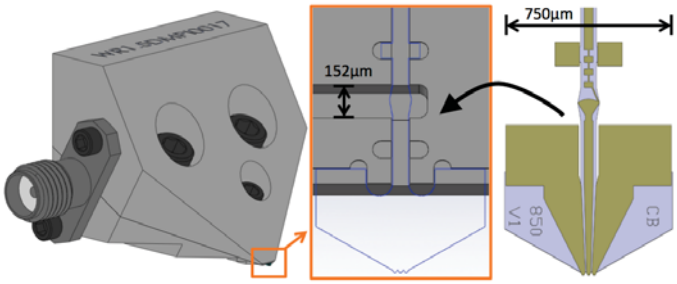

Figure 1. Self-aligned drop-in assembly process for micromachined on-wafer probe. The WR-1.2 waveguide channel height is 152 μm.

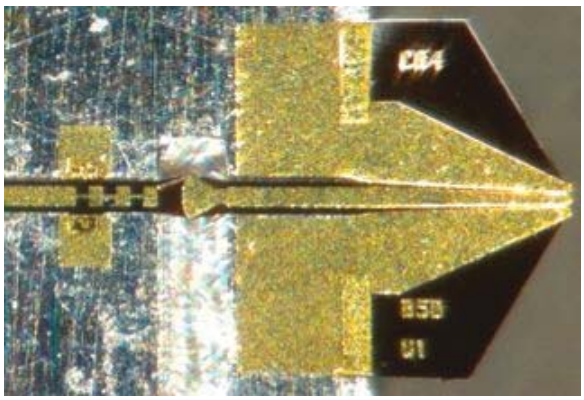

Figure 2. Micrograph of a WR-1.2 probe chip mounted in one half of the split-block waveguide housing, prior to being clamped in place. The E-plane probe is seen suspended over the waveguide channel.

II. Probe Design

The RF design of the probe chip mainly consists of two transitions, one from WR-1.2 rectangular waveguide to a substrate-supported rectangular coaxial transmission line, and a second from the rectangular coaxial transmission line to coplanar waveguide (CPW), which extends down to the tips. An example photo of a fabricated probe of this type is shown in Fig. 2. Near the center of the photo, the waveguide radial probe is suspended in the WR-1.2 waveguide channel, with the transition from rectangular coaxial to the CPW tips shown to the right. In a configuration similar to that described in [8], the radial probe is connected on the left side of the waveguide to a microstrip RF choke filter. This serves as a DC signal line, allowing DC bias to be passed through the probe tips to the DUT.

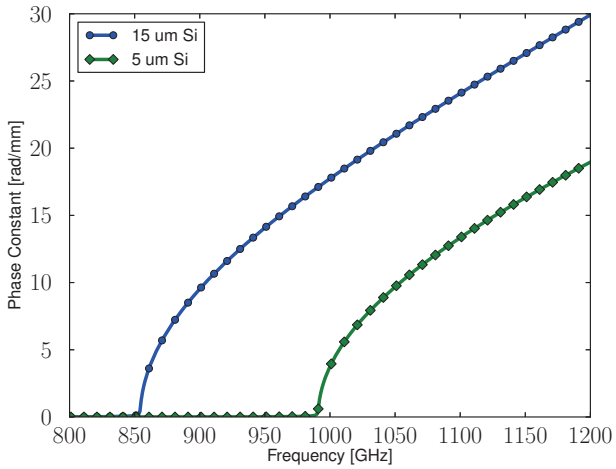

Figure 3. Cutoff frequency of first spurious mode in the coaxial channel for 15um and 5um Si substrates.

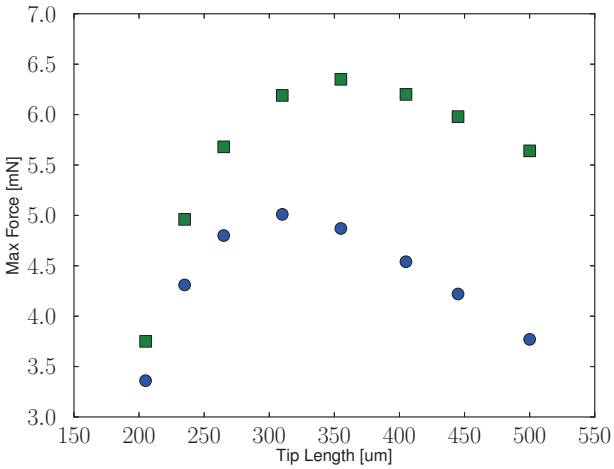

Figure 4. Maximum force generated at probe tip for various tip geometries. The circle markers indicate a 750 μm wide and the square markers indicate a 1500 μm wide tip.

The design process begins with the choice of the silicon substrate thickness, as it has a substantial effect on both the electrical and mechanical properties of the probe. The substrate must be thick enough that the tips can generate sufficient force for good electrical contact. However, for a low-loss design, it must also be thin enough to ensure that spurious substrate modes do not propagate in the rectangular coaxial transmission line channel. To check the cutoff frequency of the first substrate mode, a plot of its phase constant is generated through finite element simulations in Ansoft HFSS for both 15 μm and 5 μm silicon substrates. As shown in Fig. 3, the first spurious mode for a 15 μm substrate begins propagating within the WR-1.2 band, while for a 5 μm substrate, it does not.

As a result of choosing a thinner substrate, the spring constant of the tip will be reduced. It was established in [5] and [6] that a low-resistance contact is formed between the tip and the probed substrate with a contact force of approximately 1 millinewton (mN) per tip. To determine if a 5 μm-thick tip is capable of generating such force, ANSYS finite element simulations were performed to determine the spring constant of the tip. A number of tip geometries were evaluated, and the results are shown in Fig. 4. While it is clear that the spring constant of the tip can be increased by either shortening or widening the tip, shortening the tip also brings the bottom of the waveguide block closer to the probed substrate. This reduces the distance the tip can deflect before the block contacts the substrate and therefore reduces the maximum force that can be generated at the tip. These competing effects lead to an optimum probe length that maximizes the potential contact force. Fig. 4 is shows that a 750 μm-wide tip can generate up to 5 mN total force, or approximately 1.7 mN per tip. In addition, the figure shows that doubling the probe tip width from 750 μm to 1500 μm increases the maximum contact force by approximately 25%.

Ansoft HFSS is used to simulate the RF response of the probe and an example simulation model is shown in Fig. 5. It consists of two wave ports, one for the WR-1.2 rectangular

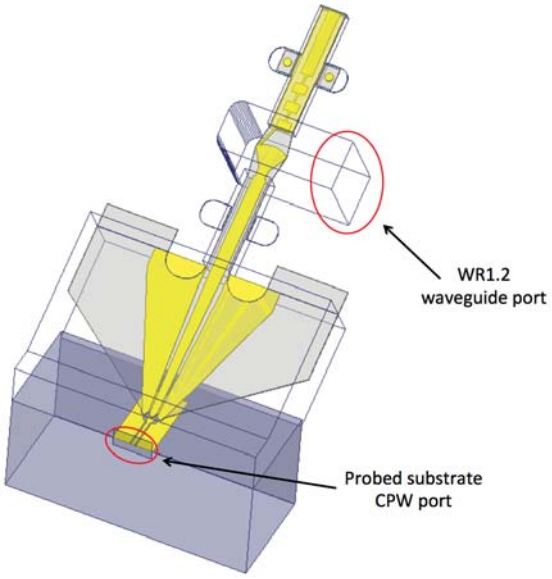

Figure 5. Full HFSS model of probe, port 1 - WR-1.2 waveguide, port 2 - probed substrate CPW.

waveguide and a second for the CPW transmission line on the probed substrate. Radiation boundaries are used around the tip to allow for radiation losses. The simulated scattering parameters (S-parameters) are shown in Fig. 6. The waveguide and CPW return loss are better than 13 dB for most of the band, and the insertion loss ranges from 2.4 to 3.8 dB. It is important to note that the simulation does not include the loss due to the 22 mm-long section of waveguide between the radial probe and waveguide flange. Not shown is the bias port isolation, which is better than 20 dB across the band.

III. Mechanical Test

When the probe chip is clamped between the two halves of the split-block housing, the tip resembles a cantilever beam. As the tip is brought into contact with the test wafer, it deflects

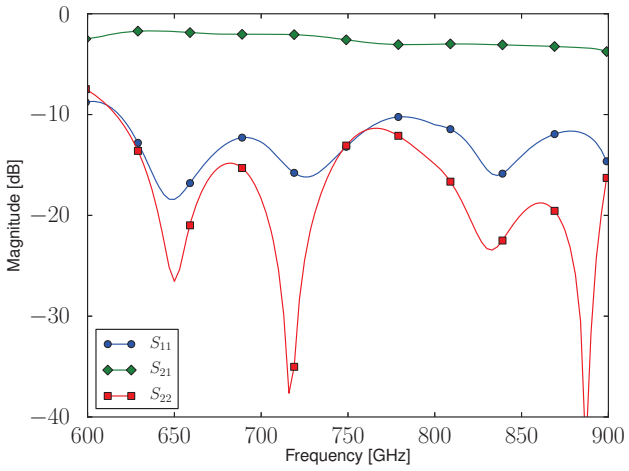

Figure 6. Simulated S-parameters of the WR-1.2 probe

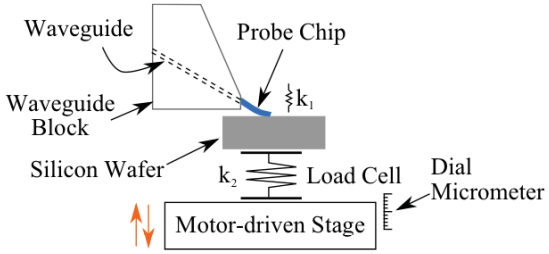

Figure 7. Mechanical test setup used to determine the effective spring constant of the probe tip.

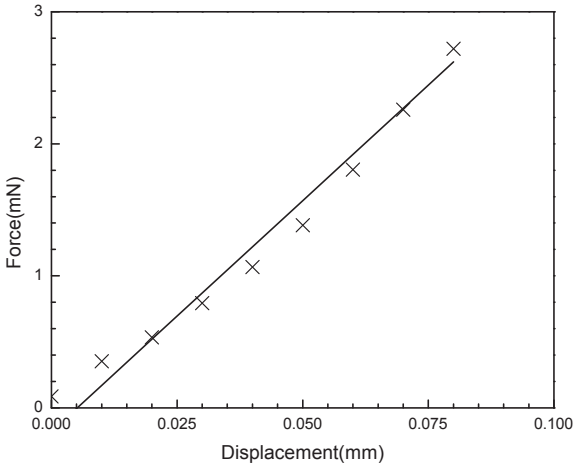

Figure 8. Measurement results of the spring constant mechanical test

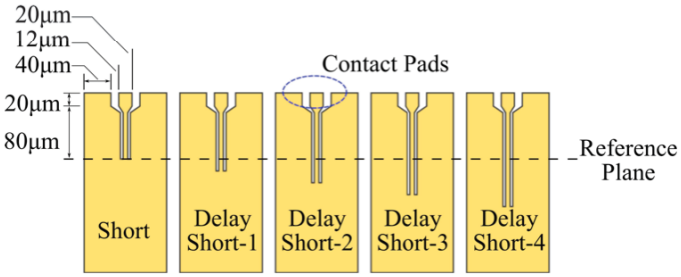

Figure 9. Layout of the CPW calibration standards. The CPW is 5/10/5 μm.

and generates a force at the contact points. To determine the effective spring constant of the tip, an experimental setup utilizing a load cell (Futek® FSH0234) and precision motor stage is used. A diagram of this setup is shown in Fig. 7. The force reading from the load cell and the position of the precision motor stage are both recorded as the test wafer is raised into contact with the probe tip. The load cell itself also deflects during this measurement. As a result, the system effectively consists of two springs connected in series. By separately measuring the spring constant of the load cell, k_2, the spring constant of the probe tip, k_1, can be determined. The experimental results are shown in Fig. 8, which indicate that the probe tip spring constant is $k_1 = 0.038 \pm 0.005$ mN/μm.

IV. RF Measurement

While the micromachined probe is designed for WR-1.2 rectangular waveguide, its S-parameters are first measured in the WR-1.5 band due to the current configuration of our probe test station. The measurement setup consists of a one-port WR-1.5 frequency extension unit from Virginia Diodes Inc. (VDI WR1.5 VNAXTXRX) in conjunction with a Rhode & Schwartz ZVA-40 network analyzer. The upper half of the probe's response, from 750 to 900 GHz, will be characterized with a VDI WR-1.0 frequency extension unit. By utilizing a two-tier calibration technique, the full two-port S-parameters can be determined. This method consists of performing calibrations at the two reference planes of interest. In this case, the first reference plane is at the WR-1.5 waveguide test port and the second is along a CPW transmission line on the calibration test wafer.

The waveguide calibration is performed using a waveguide short, delay short, and load. After the waveguide calibration is completed, the probe is attached to the waveguide test port and the second-tier calibration is performed on-wafer. The on-wafer calibration standards consist of a CPW short and a series of four CPW delay shorts, as shown in Fig. 9. The reference plane is offset from the contact pad by 80 μm, and each delay short is 18 μm longer than the previous. Electrically, this 18 μm length represents 35° at 625 GHz so that the longest delay short is 140° long at 625 GHz. The substrate for the on-wafer calibration standards is 380 μm-thick high resistivity silicon (>10 kΩ·cm). Note that at the time of measurement, a calibration wafer had not yet been specifically fabricated for the WR-1.2 probes. The contact pads were designed for a probe tip pitch of 30 μm, while the WR-1.2 probe tip pitch is 25 μm.

The reflection coefficients of the on-wafer CPW delay shorts, Γ_{ds}, are related to the reflection coefficients measured at the waveguide test port, Γ_{wg}, and the embedding network coefficients, e_{ij}, by the well-known bilinear transform,

$$\Gamma_{wg} = e_{11} + \frac{e_{21}e_{12}\Gamma_{ds}}{1 - e_{22}\Gamma_{ds}}$$

In this case, the embedding network represents the probe itself, and the coefficients e_{ij}, are the S-parameters of the probe. By

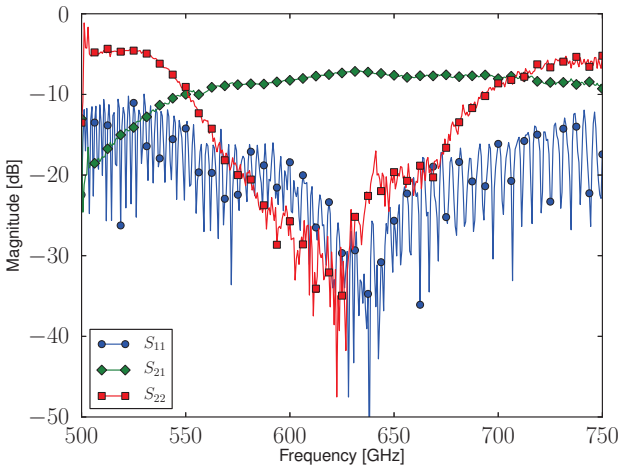

Figure 10. Measured S-parameters of the WR-1.2 probe in the WR-1.5 band.

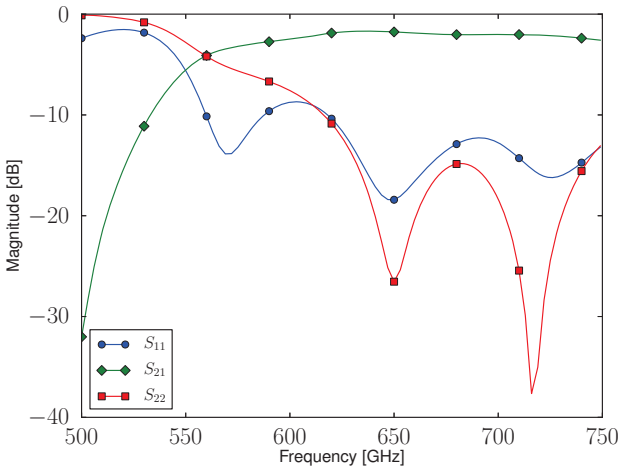

Figure 11. Simulated s-parameters of the WR-1.2 probe in the WR-1.5 frequency band

noting that the probe is a reciprocal network, the full two-port S-parameters of the probe can be obtained.

Given that the *S*-parameter measurements were taken with a one-port WR-1.5 frequency extension unit, the measurement only captures the lower half of the probe's designed response, from 600 to 750 GHz. The measured data are shown in Fig. 10. The waveguide return loss is better than 10 dB across the band and the insertion loss is better than 9 dB for the lower half of the WR-1.2 band. The measured CPW return loss, however, is greater than expected above 675 GHz. This may be due to the pitch mismatch between the probe tips and the calibration standards, and it is currently under investigation. To make a comparison to the out-of-band response, an additional simulation was run and the result is shown in Fig. 11. While the simulation does not account for the waveguide loss, it can be seen that the measured and simulated insertion losses are qualitatively similar. Both are relatively flat across the band and begin to roll off at approximately 550 GHz.

V. Conclusion

An on-wafer probe designed for use with WR-1.2 waveguide has been designed and fabricated. Initial tests show insertion loss of better than 9 dB for the lower half of the WR-1.2 band. The upper half of the probe's frequency response will be characterized using a Virginia Diodes Inc. WR-1.0 frequency extension unit.

Acknowledgment

The authors would like to thank Dr. John Albrecht of DARPA, Dr. Alfred Hung of ARL, and Dr. Bill Deal of Northrop Grumman. This work was supported by the U.S. Army National Ground Intelligence Center (NGIC) under contract W911W5- 06-R-0001 and the DARPA THz Electronics Program and Army Research Laboratory under DARPA Contract no. HR0011-09-C-0062 under a sub-contract from Northrop Grumman. The views, opinions, and/or findings contained in this article are those of the authors and should not be interpreted as representing the official views or policies, either expressed or implied, of the Defense Advanced Research Projects Agency or the Department of Defense. Approved for Public Release, Distribution Unlimited.

References

[1] P. Siegel, "Terahertz technology," *Microwave Theory and Techniques, IEEE Transactions on*, vol. 50, no. 3, pp. 910–928, Mar. 2002.

[2] V. Radisic, K. Leong, X. Mei, S. Sarkozy, W. Yoshida, and W. Deal, "Power amplification at 0.65 THz using InP HEMTs," *Microwave Theory and Techniques, IEEE Transactions on*, vol. 60, no. 3, pp. 724 –729, Mar. 2012.

[3] W. Deal, K. Leong, V. Radisic, S. Sarkozy, B. Gorospe, J. Lee, P. Liu, W. Yoshida, J. Zhou, M. Lange, R. Lai, and X. Mei, "Low noise amplification at 0.67 THz using 30 nm InP HEMTs," *Microwave and Wireless Components Letters, IEEE*, vol. 21, no. 7, pp. 368 –370, Jul. 2011.

[4] A. Fung, L. Samoska, D. Pukala, D. Dawson, P. Kangaslahti, M. Varonen, T. Gaier, C. Lawrence, G. Boll, R. Lai, and X. Mei, "On-wafer s-parameter measurements in the 325-508 GHz band," *Terahertz Science and Technology, IEEE Transactions on*, vol. 2, no. 2, pp. 186 –192, Mar. 2012.

[5] T. Reck, L. Chen, C. Zhang, A. Arsenovic, C. Groppi, A. Lichtenberger, R. Weikle, and N. Barker, "Micromachined probes for submillimeter-wave on-wafer measurements-part I: Mechanical design and characterization," *Terahertz Science and Technology, IEEE Transactions on*, vol. 1, no. 2, pp. 349–356, Nov. 2011.

[6] ——, "Micromachined probes for submillimeter-wave on-wafer measurements-part II: RF design and characterization," *Terahertz Science and Technology, IEEE Transactions on*, vol. 1, no. 2, pp. 357–363, Nov. 2011.

[7] R. Bass, A. Lichtenberger, R. Weikle, S. Pan, E. Bryerton, and C. Walker, "Ultra-thin silicon chips for submillimeter-wave applications," in *Fifteenth International Symposium on Space THz Technology*, 2004, pp. 392–399.

[8] C. Risacher, V. Vassilev, A. Pavolotsky, and V. Belitsky, "Waveguide-to-microstrip transition with integrated bias-T," *Microwave and Wireless Components Letters, IEEE*, vol. 13, no. 7, pp. 262 –264, Jul. 2003.